in P. Pasini, C. Zannoni and S. Zumer, (editors),
Computer Simulations of Liquid Crystals and Polymers, Kluwer, Dordrecht (2005)

LATTICE SPIN MODELS OF POLYMER-DISPERSED LIQUID CRYSTALS

Cesare Chiccoli, Paolo Pasini
Istituto Nazionale di Fisica Nucleare, Sezione di Bologna,
Via Irnerio 46, I-40126, Bologna, ITALY
Paolo.Pasini@infn.bo.it

Gregor Skačej, Slobodan Žumer
Oddelek za fiziko, Univerza v Ljubljani,
Jadranska 19, SI-1000 Ljubljana, SLOVENIA
slobodan.zumer@fmf.uni-lj.si

Claudio Zannoni
Dip. di Chimica Fisica ed Inorganica, Università di Bologna,
Viale Risorgimento 4, I-40136, Bologna, ITALY
Claudio.Zannoni@cineca.it

Abstract Monte Carlo simulations of lattice spin models are a powerful method for the investigation of confined nematic liquid crystals and allow for a study of the molecular organization and thermodynamics of these systems. Investigations of models of polymer-dispersed liquid crystals are reviewed devoting particular attention to the calculation of deuterium NMR spectra from the simulation data.

Introduction

Lattice spin systems are the simplest models used for the investigation of liquid crystals by means of computer simulations [1] and were introduced in this field by Lebwohl and Lasher (LL) [2]. After their pioneering work a large amount of simulations has been done on generalizations of the LL model [1], even though in the last few years more realistic potentials, like the Gay-Berne one [3] or its generalizations [4], have become popular. Anyhow, as long as the properties of interest are purely orientational, there are several advantages in using simple lattice models

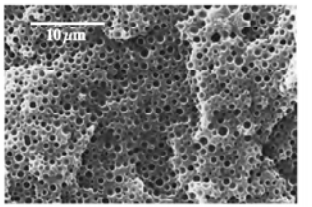

Figure 1. **Scanning electron microscope photograph of a PDLC sample with the** liquid crystal removed (from Ref. [8]). The average droplet radius is approximately 400 nm.

(with respect to potentials with translational degrees of freedom), particularly the possibility of performing simulations on a large number of particles. As an alternative, using smaller lattices it is possible to investigate potentials for more complicated systems depending on additional parameters, for example associated with changes in boundary conditions and field strengths, over a wide range of state points. For instance, the Monte Carlo (MC) simulation method was applied to studies of confined nematics where it is important to perform the calculations under a variety of different conditions [1]. As technical applications of confined liquid crystals are numerous, the need to understand and predict various experimental situations makes the simple spin models a convenient and flexible tool to simulate realistic situations. In particular, we have shown that this technique is useful in investigating droplets with fixed (homeotropic and planar) surface alignment [5, 6] mimicking polymer-dispersed liquid crystals (PDLC) [7]. Here we give a brief resume of the method and a short review of the main results obtained from the simulations of nematic droplets.

1. Polymer-dispersed liquid crystals

Polymer-dispersed liquid crystals (PDLC) [7] are materials that consist of microscopic nematic droplets, with typical radii from a few hundred Ångström to more than a micron, embedded in a polymer matrix (see Fig. 1). These systems are interesting both for technical applications and for an understanding of the behavior of mesophases in a confined environment. PDLC droplets also represent practical realizations of systems exhibiting topological defects of interest in many fields

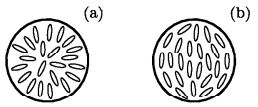

Figure 2. A schematic representation of the molecular ordering inside a PDLC droplet in the nematic phase; (a) radial, (b) bipolar.

of physics [9, 10]. Various experimental works have considered different boundary conditions (see Fig. 2) at the droplet surface, for example radial [11, 12], axial [12], toroidal [13] and bipolar [11, 12, 14] ones, depending on the polymer matrix chosen, and on the preparation methods. The resulting molecular organization inside a PDLC droplet stems from a competition between surface boundary condition effects, the nematic ordering inside the system, and thermal disorder. Additional effects of interest come from the application of an external electric or magnetic field [11]. From the theoretical point of view these systems have been studied by means of elastic continuum approaches [7] and by Monte Carlo computer simulations of lattice models [1].

MC simulations have been used to study PDLC in a variety of physical situations: for different boundary conditions [5, 6] and anchoring strengths at the nematic/polymer interface [5, 6], as well as for different strengths of the external field [6]. Methodologies to calculate deuterium NMR line shapes and textures observable in polarized light experiments corresponding to the microscopic configurations found have also been developed [1, 15, 16]. Here we describe how to bridge the gap between simulations and experimental investigations performed on the same systems.

2. The simulation method

As already mentioned, we deal with systems defined on a simple cubic lattice where the N particles (spins) interact through a pair potential of the form

$$U_{ij} = -\epsilon_{ij} P_2(\cos\beta_{ij}) = -\epsilon_{ij}\left[\frac{3}{2}(\mathbf{u}_i \cdot \mathbf{u}_j)^2 - \frac{1}{2}\right]. \qquad (1)$$

Here ϵ_{ij} is a positive constant for nearest neighbor spins i and j (zero otherwise), P_2 is the second-rank Legendre polynomial, and β_{ij} is the angle between the three-dimensional unit vectors $\mathbf{u}_i$ and $\mathbf{u}_j$ located at the lattice sites (particles are assumed to have uniaxial symmetry). The LL model gives a good representation of the orientational properties

of a real nematic, showing a weakly first order nematic-isotropic (NI) phase transition (at a scaled temperature $T^*_{NI} = k_B T_{NI}/\epsilon = 1.1232$) [17, 18], a reasonable dependence of the orientational order parameter $\langle P_2 \rangle$ against temperature, and even diverging pretransitional effects, as also found for real nematics just above T^*_{NI}. We have suggested [6] that the model works so well because a "spin" represents a closely packed group of molecules, rather than a single particle, and that these microdomains maintain their local structure at various temperatures and even across the nematic-isotropic phase transition [5]. As a special case these domains could comprise just one molecule but it seems more realistic to assume that they typically include up to a hundred of particles.

The configuration of the system is given by the set of spin orientations. To update the lattice we use a standard Metropolis Monte Carlo procedure [19], and a new configuration is then generated by choosing a particle at random for a trial move at every cycle using a random shuffling algorithm [17]. The new orientation of the chosen particle is generated by a controlled variation from the old one using the Barker-Watts technique [20], to achieve a rejection ratio not too far from 0.5. A certain number of cycles (a cycle is a set of N attempted moves) is performed, and any property of interest (e.g., A) is evaluated at every cycle or every few cycles. The observable value $\langle A \rangle$ is then obtained as an average over these instantaneous values. For each simulation we routinely calculate energy, heat capacity, nematic second-rank order parameter and pair correlation coefficients. In addition, order parameters suitable to quantify a particular type of ordering for the different cases are introduced and calculated, as outlined in the following sections. Moreover, the MC technique was shown to be a powerful method also for the simulation of experimental observables, like polarized light textures [1] or NMR spectra [1, 15, 16, 21].

2.1 The PDLC simulation model

The properties of the nematic at the interface depend on the characteristics of the surface in contact with the liquid crystal, and the task of defining and including the boundary conditions in the spin model is hence fundamental for a simulation of a confined system. The PDLC model consists of an approximately spherical sample $\mathcal{S}$ carved from a cubic lattice with spins interacting with the LL potential, as given in Eq. (1), while the surface effects are modeled with a layer of outside "ghost" spins, $\mathcal{G}$, which are kept frozen during the simulation. The liquid crystal particles at the interface tend to be ordered according to the orientation of the "ghost" neighbor molecules in the outside environ-

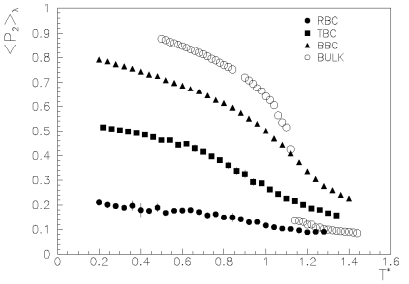

Figure 3. Nematic order parameter $\langle P_2\rangle_\lambda$ versus temperature for the radial, toroidal and bipolar boundary conditions ($J = 1$) and for the bulk. All the results have been obtained from simulations of a droplet carved from a $10 \times 10 \times 10$ lattice.

ment, through a coupling depending on the anchoring strength. This ordering propagates from the surface layer of the liquid crystal towards the droplet center. The coupling between nematic and "ghost" spins can be varied to model the effect of different surface materials, i.e.,

$$U_{ij} = -\epsilon_{ij} J \left[\frac{3}{2}(\mathbf{u}_i \cdot \mathbf{u}_j)^2 - \frac{1}{2}\right], \qquad \text{for} \qquad i \in \mathcal{S}, j \in \mathcal{G}, \tag{2}$$

where the parameter J accounts for the strength of anchoring at the polymer surface. When the interaction between two neighbors, one on the surface of the nematic droplet and one belonging to the outside matrix, is the same as that between two liquid crystal spins then $J = 1$, while $J = 0$ would correspond to a droplet in vacuum.

2.2 Molecular ordering

To examine the ordering inside the microdroplet, various second-rank order parameters are calculated for the systems to be investigated. The global second-rank order parameter, $\langle P_2\rangle_\lambda$, is obtained as the largest eigenvalue from the diagonalization of the ordering matrix averaged over the whole sample and MC cycles [1]. $\langle P_2\rangle_\lambda$ then quantifies the nematic order with respect to a hypothetical global director. In Fig. 3 the parameters $\langle P_2\rangle_\lambda$ for the radial, bipolar, and toroidal boundary conditions are shown together with the bulk behavior, as obtained from simulations in a bulk system of the same size. From the $\langle P_2\rangle_\lambda$ curves it can be deduced that the nematic-isotropic phase transition is suppressed for small

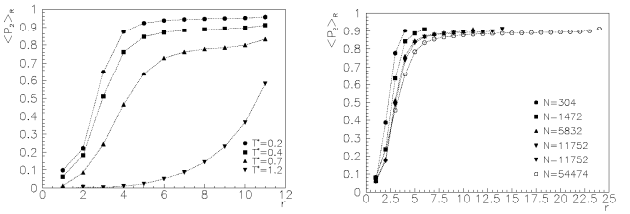

Figure 4. Radial order parameter $\langle P_2\rangle_R$ for a nematic droplet with radial boundary conditions plotted against the distance, in lattice units, from the center of the sphere. Results for a $N = 5832$ particle droplet at some scaled temperatures (*left*) and for different system sizes at temperature $T^* = 0.2$ (*right*).

enough confined systems, as confirmed by the heat capacity behavior [5]. Moreover, we have found it useful to define some order parameters more appropriate to each special case. For example, in case of radial boundary conditions, it is not possible to distinguish between a perfectly ordered radial configuration and a completely disordered system just from the value of $\langle P_2\rangle_\lambda$. We have then defined a radial order parameter [5]

$$\langle P_2\rangle_R = \frac{1}{N}\sum_{i=1}^{N} P_2(\mathbf{u}_i \cdot \mathbf{r}_i) \tag{3}$$

where $\mathbf{r}_i$ is the radial vector of the ith spin. For a perfect "star" configuration $\langle P_2\rangle_R = 1$. It is also possible to divide the droplet into concentric shells and calculate relevant quantities within such regions, so as to monitor the variation of the ordering on going from the center to the border of the system. As an example, the behavior of $\langle P_2\rangle_R$ with respect to the distance from the droplet center r is reported in Fig. 4 at some selected temperatures (left plate), and for different droplet sizes at $T^* = 0.2$ (right plate). These results show a nematic ordered core at the center of the droplet consistent with a ring disclination [22].

Following the same line of thoughts, it is possible to define a configurational order parameter, $\langle P_2\rangle_C$, which tends to one for a configuration perfectly ordered according to the idealized structure induced by the boundary conditions used:

$$\langle P_2\rangle_C = \frac{1}{N}\sum_{i=1}^{N} P_2(\mathbf{u}_i \cdot \mathbf{c}_i). \tag{4}$$

Here $\mathbf{c}_i$ denotes the direction corresponding to the local alignment induced by the surface. For example, in the bipolar case $\mathbf{c}_i$ is a local meridian that lies on the plane defined by the droplet axis (z-axis) and the radial vector $\mathbf{r}_i$ of the particle while being perpendicular to $\mathbf{r}_i$ itself.

It is also convenient to calculate the local second-rank order parameter S, again obtained by diagonalizing the local ordering matrix. Contrary to the global second-rank order parameter $\langle P_2 \rangle_\lambda$ introduced above, here the ordering matrix is calculated for each lattice site separately and averaged over MC cycles only [15, 16]. Therefore the resulting ordering matrix is "MC time"- rather than ensemble-averaged. After diagonalization, the eigenvalues with largest absolute values are identified as the local S. These can then be averaged either over the whole droplet or within spherical shells [e.g., to yield $S(r)$ profiles]. Further, in presence of external fields additional order parameters can be defined and will be introduced later.

Finally, to understand the effect of the size dependence in the model, samples of different sizes (from 304 to 54474 spins) have been investigated [10]. The similarity in the behavior of properties calculated for different sample sizes supports the argument that each of the spins could really be a microdomain of up to 100 particles, and that our results also are applicable to droplets in the micron size that have been investigated experimentally [7]. Note that a full rescaling of order parameter profiles is not possible in the vicinity of topological defects (present, e.g., in radial droplets), but the defect size — given by the non-scalable nematic correlation length — is usually too small to significantly affect the overall behavior of the system.

3. ^{2}H NMR

Deuterium nuclear magnetic resonance (^{2}H NMR) [8, 11, 23, 24] is a powerful experimental technique that is most frequently applied to investigate poly-mer-dispersed liquid crystals (PDLCs). It is very convenient for the study of such heterogeneous systems since using deuterated nematics the resulting spectra only give direct information on the behavior of the liquid crystal confined to spherical cavities inside the non-deuterated polymer matrix. Further, it is applicable also to small, i.e., submicron droplets, where optical methods fail to yield useful information because the light wavelength is too large compared to the droplet diameter. ^{2}H NMR spectra provide information about the orientational molecular ordering inside nematic droplets, including director configurations and dynamic processes such as molecular fluctuations and diffusion.

In the bulk isotropic phase, the ^{2}H NMR spectrum of a nematic selectively deuterated at one position consists of a single line whose position in the spectrum is determined by the Zeeman splitting of deuteron energy levels in the spectrometer magnetic field and whose width is well below 100 Hz. Since deuterons possess a nonzero quadrupolar moment, there is an additional perturbative contribution to their energy levels coming from quadrupolar interactions between them and the electric field gradient (EFG) of the C-D bonds in nematic molecules. These anisotropic perturbative contributions are completely averaged out by molecular motions in the isotropic, but not in the nematic phase. Indeed, once in the nematic phase, the single narrow line splits into a doublet, the frequency splitting now being typically of the order of ~ 100 kHz. It depends on the relative orientation of the EFG tensor symmetry axis (which is related to the orientation of the long molecular axis $\mathbf{a}$ and the director $\mathbf{n}$) and the direction of the external magnetic field $\mathbf{B}$. For uniaxial nematics this splitting is given by [7, 25, 26]

$$\omega_Q(\mathbf{r}) = \pm \delta\omega_Q \, S(\mathbf{r}) \left| \frac{3}{2} \cos^2 \theta(\mathbf{r}) - \frac{1}{2} \right| , \tag{5}$$

where $\delta\omega_Q$ is its maximum value (proportional to the quadrupolar tensor anisotropy), $S(\mathbf{r})$ is the local uniaxial nematic scalar order parameter defined by the average $S(\mathbf{r}) = \frac{1}{2}[3\langle(\mathbf{n}(\mathbf{r}) \cdot \mathbf{a})^2\rangle - 1]$, and $\theta(\mathbf{r})$ is the angle between the local director $\mathbf{n}(\mathbf{r})$ and the magnetic field $\mathbf{B}$. In confined nematics, e.g., in PDLCs, the director orientation will change with position, $\mathbf{n} = \mathbf{n}(\mathbf{r})$ reflecting the boundary conditions imposed by the polymer matrix. Consequently, the corresponding contributions to the ^{2}H NMR line splitting $\omega_Q(\mathbf{r})$ will depend on $\mathbf{r}$ as well. Since the NMR spectrum corresponds to the overall response of all molecules in the sample, each of the director configurations $\mathbf{n}(\mathbf{r})$ appearing inside the droplet yields a specific contribution. The identification of each contribution can, however, be very problematic since also dynamic processes such as molecular fluctuations and translational diffusion affect the ^{2}H NMR line shape.

In the absence of significant molecular motion the spectra can be calculated simply as a powder-like super-imposition of the individual molecular static lines of Lorentzian shape from all over the sample. These lines are then positioned into the spectrum according to Eq. (5) as in Ref. [6]. To include also dynamic effects, such as fluctuations of molecular long axes (defining the scalar order parameter S and the director $\mathbf{n}$) and translational molecular diffusion, it is convenient to use a semi-classical approach with the time-dependent deuteron spin Hamiltonian [25] where the ^{2}H NMR line shape $I(\omega)$ is calculated as the Fourier transform of

the relaxation function $G(t)$

$$I(\omega) = \int \exp(i\omega t)\, G(t)\, dt, \tag{6}$$

where $G(t)$ is generated as

$$G(t) = \exp(i\omega_Z t)\Big\langle \exp\,(i \int_0^t \Omega_Q[\mathbf{r}_i(t'), t']\, dt')\Big\rangle_i. \tag{7}$$

Here ω_Z denotes the Zeeman frequency, while the brackets $\langle ... \rangle_i$ stand for the ensemble average over all molecules in the sample. The instantaneous resonance frequency of the ith molecule with coordinates $\mathbf{r}_i$ is given by $\omega_Z + \Omega_Q[\mathbf{r}_i(t'), t']$, where $\Omega_Q[\mathbf{r}_i(t'), t'] = \pm\delta\omega_Q[\frac{3}{2}(\mathbf{u}_i \cdot \mathbf{B}/B)^2 - \frac{1}{2}]$. It depends on the instantaneous molecular orientation (given by $\mathbf{u}_i$) that is constantly changing during the NMR experiment [15]. Calculating $G(t)$, it is assumed that the deuteron spin Hamiltonian is secular and hence excludes deuteron spin flips as the molecular orientation varies.

Neglecting for the moment translational diffusion, we have $\mathbf{r}_i \neq \mathbf{r}_i(t')$ and $\Omega_Q = \Omega_Q(\mathbf{r}_i, t')$. The time dependence in Ω_Q is then caused solely by fluctuations of molecular long axes, keeping molecular positions fixed. To simulate such a dynamics we calculated spectra using the data from 1024 successive MC simulation steps. The characteristic time scale for long axis orientational fluctuations t_F is in a typical liquid crystal $\sim 10^{-8}$ s [27]. The dynamics of MC simulations is determined by the arbitrary molecular evolution process chosen (in contrast to molecular dynamics simulations), so the time scale assigned to fluctuations generated by this technique does not necessarily have to match with the natural time scale indicated above. However, the update process we have adopted here moves one molecule at a time for a certain angular step and is thus a plausible physical evolution process. In this sense, we can map the MC dynamics onto a plausible real one, apart from for an arbitrary time unit. Including also the translational diffusion, we have $\mathbf{r}_i = \mathbf{r}_i(t')$, too. The typical time scale for a diffusion yielding a displacement for one molecular length (~ 1 nm) is also of the order of $t_D \sim 10^{-8}$ s [27]. It is, however, more relevant to know the time t'_D needed for a molecular diffusion to yield a displacement over which the average molecular orientation [i.e., the director field $\mathbf{n}(\mathbf{r})$] changes considerably. This distance obviously varies with the system size, i.e. the droplet radius R, so the relevant diffusion time t'_D can become much larger than t_D. In other words, in smaller droplets the effects of translational diffusion on the spectra can be much more important than in larger ones.

In order to estimate how dynamic processes influence the spectra, it is necessary to compare their typical time scales to the characteristic NMR

time scale $t_0 \approx 2\pi/\delta\omega_Q$, which, for the deuterium quadrupolar splitting in the nematic phase, is of the order of $\sim 10^{-5}$ s. If the molecular motion is sufficiently slow on the NMR time scale t_0, the spectra can be calculated as $I(\omega) = \langle\delta[\omega - \omega_Z - \omega_Q(\mathbf{r}_i)]\rangle_i$ [11], i.e., it is possible to use the static approach used in Ref. [6]. If, at the other extreme, the motion is very fast on the t_0 scale, the spectrum is completely motionally averaged and now consists of a single line $I(\omega) = \delta[\omega - \omega_Z - \langle\omega_Q(\mathbf{r}_i)\rangle_i]$ which is positioned at an average frequency $\langle\omega_Q(\mathbf{r}_i)\rangle_i$ [11].

First we have systematically calculated the NMR spectra for different director configurations in nematic droplets, proceeding from the static limit to the limit of completely motionally averaged spectra, in order to find out to which extent diffusive processes smear the spectra and thus make the identification of director configurations impossible. To see this effect, a number of simplifying assumptions, described later, has to be invoked. To ensure being well inside the nematic phase, the reduced temperature $T^* = k_B T/\epsilon$ was set to $T^* = 0.8$ (note that the nematic-isotropic transition for the LL model occurs only at $T^*_{NI} = 1.1232$). Further, in all cases the strength of the coupling between nematic and ghost spins was chosen to be $J = 1$, which implies that anchoring is rather strong. Note also that in Eq. (1) we have assumed no coupling between the spectrometer magnetic field and the molecular orientation, which is appropriate when the magnetic coherence length is much larger than the droplet diameter, i.e., when the external field is weak enough not to induce any alignment in the droplet in itself.

3.1 Orientational fluctuations

Let us first consider spectra in the absence of translational diffusion, or, equivalently, spectra of large enough nematic droplets (with $R \gg \sqrt{6Dt_0}$, where D is the diffusion constant) in which this kind of molecular motion is not very influential. The only relevant molecular dynamics is now caused by fluctuations of long molecular axes $\mathbf{a}$ around the director $\mathbf{n}$. In order to obtain a spectrum with a sufficient resolution, it is necessary to simulate a relaxation signal $G(t)$ that is long enough, i.e., lasting for several NMR cycles of duration t_0 each. Comparing the time scales of molecular fluctuations and NMR, i.e., t_F and t_0, it is evident that there should be about 10^3 molecular fluctuations per NMR cycle. This relation between t_0 and t_F did not allow us to generate a sufficiently long $G(t)$, as, for technical reasons, we only had the data for 1024 successive MC spin configurations available. Therefore, generating $G(t)$ we decided to update the spin configuration from the MC data less frequently than required by the natural time scale t_F in order to cover

a long enough period in time. This approximation is not of essential importance given the already mentioned arbitrariness in the MC time scale.

In the diffusion-less limit we updated the spin configurations inside the nematic droplet 8 times per NMR cycle, which is much less than the natural scale given above. This enabled us then to generate a $G(t)$ signal whose length is $128\,t_0$, yielding spectra with a resolution of 256 points in the relevant (nonzero) part of the spectrum. It is possible to check whether this frequency of configuration sampling is sufficient or not, by comparing the scalar order parameter S deduced from the NMR spectra and from the MC data itself. As the resulting spectra show some "noise" because of the relatively small number particles within the droplet ($N = 5832$), a convolution with a Gaussian kernel of width $0.04\,\delta\omega_Q$ has been performed to smoothen the spectra. For $\delta\omega_Q \sim 2\pi \times 100$ kHz the kernel width equals $\sim 2\pi \times 4000$ Hz, which is well above the natural line width, typically given by $\sim 2\pi \times 100$ Hz.

In the following we consider nematic droplets with radial and bipolar boundary conditions. According to Eq. (5), the full width of a doublet in the spectrum equals $2\delta\omega_Q S$. In the perfectly aligned nematic phase with $S = 1$ the spectrum width amounts to $2\delta\omega_Q$, but as soon as dynamic effects are taken into account, the spectrum is narrowed, and molecular fluctuations effectively yield $S < 1$. The spectrum of, e.g., the radial droplet, in which molecular orientations are distributed isotropically over the whole solid angle, is equivalent to the Pake-type [25] powder spectrum consisting of two asymmetric peaks positioned at $\omega_Z \pm \frac{1}{2}\delta\omega_Q S$ (see the top curve in Fig. 5, left). Therefore it is possible to deduce the value of S from the actual position of these peaks: in our case $S \approx 0.72 \pm 0.02$. This is in very good agreement with the value $S \approx 0.73$ directly obtained from the MC data by diagonalizing the "MC time"-averaged ordering matrix for each of the spins and averaging the largest eigenvalues obtained in this way over the whole droplet. This shows that even the limited sampling of MC structures still reproduces the effect of molecular fluctuations sufficiently well.

The spectrum of the bipolar droplet in the no-diffusion limit differs considerably from that of the radial droplet. If the NMR magnetic field $\mathbf{B}$ is applied along the z-axis (i.e., the symmetry axis of the droplet), it still has two asymmetric peaks, which, however, are now located approximately at $\omega_Z \pm \delta\omega_Q S$. This reveals that indeed most of the molecules are aligned parallel to $\mathbf{B}$ (see the top curve in Fig. 5, right. Evaluating S from the peak positions gives $S \approx 0.74 \pm 0.02$, while calculating S directly from the MC data yields $S \approx 0.76$. Again the agreement of the two estimates is good. In general, bipolar symmetry axes in droplets of

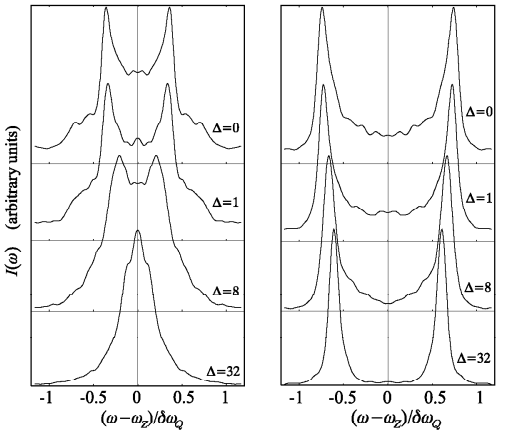

Figure 5. ^{2}H NMR spectra of the radial (*left*) and bipolar droplet (*right*) for different values of the diffusion parameter Δ: $\Delta = 0$ corresponds to the no-diffusion limit, while $\Delta = 32$ corresponds to the fast diffusion limit. *Radial droplet:* The Pake-type powder spectrum obtained for $\Delta = 0$ collapses into a single line centered at zero quadrupolar splitting for $\Delta = 32$. *Bipolar droplet:* The magnetic field is aligned along the bipolar symmetry axis, which results in a spectrum consisting of two lines both in absence of diffusion and in the fast diffusion limit.

a PDLC sample can have arbitrary spatial orientations. Summing up contributions originating from droplets from all over the sample then yields a spectrum similar to the Pake-type powder spectrum [23] (an example will be shown in the last Section). If, however, the process of nematic droplet formation in a polymer matrix has occurred in a sufficiently strong external field, the bipolar droplet axes are aligned along the field direction. This frozen-in alignment can be retained also after the field has been switched off [11], which then corresponds to the case considered here. We further assume the direction of the spectrometer magnetic field to coincide with the bipolar droplet axes.

3.2 Translational diffusion

In addition to fluctuations of the long molecular axes we would now like to include also translational molecular diffusion into the analysis. Let us consider, for simplicity, the case in which the diffusion is characterized by a single motional constant (the diffusion tensor is isotropic), i.e., the probability for a molecular diffusion does not depend on the local orientation of the director. In a bulk unconstrained nematic phase the diffusion anisotropy can be typically up to $D_{||}/D_{\perp} \approx 2$, with $D_{||}$ being measured along the director and $D_{\perp}$ perpendicular to it [11, 28]. Our tests indicate, however, that the inclusion of anisotropic diffusive process into the simulation alters the spectra only negligibly. Moreover, in a thin subsurface layer translational diffusion is affected by the presence of the confining substrate as well [29]. For now, however, we are going to ignore spatial inhomogeneities in the diffusive process and the study of these effects will be postponed until the last Section.

Isotropic translational diffusion has been simulated by a simple random walk process in which each spin — representing one or more nematic molecules — jumps to one of its nearest neighbor sites with equal probability [11]. After the diffusion jump has been performed, the spin acquires the orientation of the local director at the new coordinates. Calculating $G(t)$ we have, like in the diffusion-less case, updated from the MC data the spin configuration inside the droplet 8 times per NMR cycle. Now additional diffusion steps have been added in between these structural updates, with their number Δ ranging from 1 to 32. In this last case the spectra are completely motionally averaged due to diffusion effects since for $\Delta = 32$ each of the spins exhibits a total of 256 jumps within the duration of one NMR cycle. This already corresponds to the fast diffusion limit with $t'_D \ll t_0$.

Consider now the case of radial boundary conditions. Fig. 5, left, shows a sequence of radial droplet spectra, ranging from the no-diffusion limit ($\Delta = 0$) to the fast diffusion limit ($\Delta = 32$). In general, for any type of boundary conditions the fast diffusion spectrum consists of two lines centered at $\omega_Z \pm |\langle\omega_Q\rangle_i|$, where the average frequency is given by $\langle\omega_Q\rangle_i - \perp\delta\omega_Q\, S\, \langle\frac{1}{2}[3\cos^2\theta(\mathbf{r}_i) - 1]\rangle_i$. If the diffusion is fast enough so that molecules diffuse through a large enough portion of the droplet, in the radial configuration where $\langle\omega_Q\rangle_i = 0$ holds, the two lines should coalesce into a central line (zero quadrupolar splitting). Inspecting the simulated spectra (the sequence in Fig. 5, left), it is evident that this indeed happens. It is possible to deduce the value of $\langle\omega_Q\rangle_i$ also directly from the MC data, yielding $\langle\omega_Q\rangle_i \approx 0.03$.

Repeating the same analysis for the bipolar droplet, we observe that the two lines in the spectrum do not merge into a single line, as just observed for the radial droplet when moving from the slow into the fast diffusion regime (Fig. 5, right). This happens because now we are dealing with an ensemble of molecules whose orientational distribution is spatially anisotropic. Hence, $\langle\omega_Q\rangle_i \neq 0$ should be expected, unless (by coincidence) the relative orientation of the external magnetic field and the majority of nematic molecules yields $\omega_Q \approx 0$ already in itself. This is, however, not the case for the spectra shown in Fig. 5, right: here $\langle\omega_Q\rangle_i = (0.61 \pm 0.02)\,\delta\omega_Q$ from the peak positions and $0.59\,\delta\omega_Q$ from the MC data.

As indicated before, diffusive processes are expected to be more important in small droplets than in large ones. Therefore it is convenient to express the limit between the slow and fast diffusion regimes in terms of the droplet size, keeping the value of the diffusion constant fixed (e.g., to $D \approx 10^{-10}$ m^2/s). This can be done since the spins used for modeling the nematic can be interpreted also as close packed clusters of several (up to ~ 100) molecules [6]. Putting the droplet radius R as an estimate for the characteristic length over which $\mathbf{n}(\mathbf{r})$ changes considerably and $t'_D \approx t_0 \approx 10^{-5}$ s give $R = \sqrt{6Dt_0} \approx 75$ nm. Hence, for this particular choice of D and t_0 in droplets with $R \gg 75$ nm diffusive effects can be neglected while in those with R below ≈ 75 nm this cannot be done.

Lining up spectra for the two different types of boundary conditions and comparing them shows that in the slow diffusion limit it is always possible to identify the radial structure because of its characteristic Pake-type spectral shape that does not depend on the direction of the external magnetic field. The spectra of the bipolar droplet, on the other hand, depend significantly on the magnetic field direction since the corresponding director configurations are anisotropic due to net molecular alignment. All these conclusions hold also in the fast diffusion regime, except that the Pake-type spectrum of the radial droplet collapses into a single line at zero splitting, again regardless of the magnetic field direction. The diffusion-averaged spectra of the bipolar structure show two peaks at nonzero splitting, unless, again, the majority of the spins is lying at a "magic" angle with respect to the magnetic field direction.

4. External field effects

In presence of an aligning external field the Hamiltonian for our model system consisting of N spins can be written as

$$U_N = -\epsilon \sum_{\langle i<j \rangle} P_2(\cos\beta_{ij}) - \epsilon\eta \sum_{i=1}^{N} P_2(\cos\beta_i), \qquad (8)$$

with $\cos\beta_i = \mathbf{f}\cdot\mathbf{u}_i$, where $\mathbf{f}$ is a unit vector in the external field direction. Further, η is a dimensionless constant describing the strength of the coupling with the external field. In the magnetic field case η is defined by $\epsilon\eta = \chi_a V_0 B^2/3\mu_0$, where B stands for the magnetic induction, $\chi_a = \chi_{||} - \chi_\perp$ is the anisotropy of the microscopic magnetic susceptibility ($||$ and $\perp$ referring to the direction of $\mathbf{u}_i$), μ_0 the permittivity of the vacuum, and V_0 the volume of space belonging to one molecule or spin (see, e.g., [6]). For $\eta > 0$ ($\chi_a > 0$) nematic molecules (particles) are aligned along $\mathbf{f}$. In order to influence the molecular alignment inside the droplet significantly, the external field has to be strong enough so that the characteristic length of the field-induced distortion — the magnetic coherence length $\xi \propto 1/B$ [28] — becomes comparable to or smaller than the characteristic dimension of the confined system, in our case simply the droplet radius R. In an experiment with an aligning magnetic field it is usually the NMR spectrometer field itself taking the role of the external field introduced in the Hamiltonian (8). Here, however, we still distinguish between the "weak" NMR spectrometer field and the "strong" external field of variable strength, responsible for the additional molecular alignment.

Note that although above we decided to refer to magnetic field effects, in a real experiment one can more easily achieve the high field strengths required to align nematic molecules by applying an electric field [8, 14, 28]. Matching aligning effects in the electric and the magnetic case, for a given nematic species one can translate any magnetic field strength (or B) into an equivalent strength of the electric field (E) [6]. In the electric case we then have $\epsilon\eta = \epsilon_a\epsilon_0 V_0 E^2/3$, where $\epsilon_a = \epsilon_{||} - \epsilon_\perp$ is the microscopic anisotropy of the dielectric constant and ϵ_0 the dielectric constant of the vacuum.

4.1 Radial droplet

We now turn to radial droplets for which, in absence of external fields (with $\eta = 0$) and for $T^* = 0.8$ the "hedgehog"-like structure is stable. As discussed above, the spectrum of the radial droplet for $\eta = 0$ is the Pake-type powder pattern consisting of two asymmetric peaks at $\pm\frac{1}{2}\delta\omega_Q S$ [25],

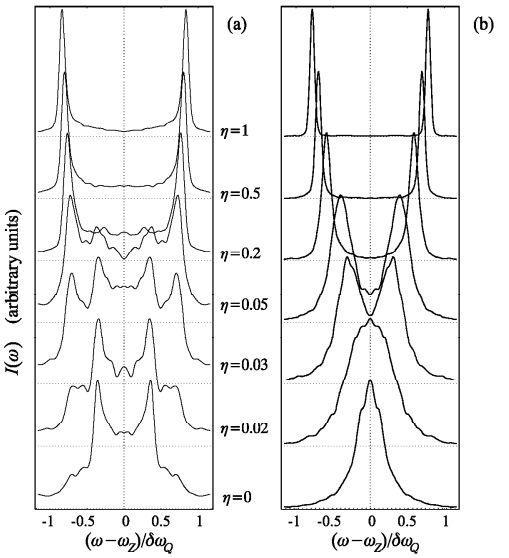

Figure 6. ^{2}H NMR spectra of the radial droplet in the nematic phase at $T^* = 0.8$ for different values of field strength η; no-diffusion limit (a), fast diffusion limit (b). A hedgehog-to-axial structural transition occurs with increasing η. All spectra have been normalized so as to obtain same peak heights.

as shown in Fig. 6 (a) for the diffusion-less case. Applying an external field with $\eta > 0$, the radial "hedgehog" structure containing a point-like defect transforms into an axially symmetric structure with a ring defect. A sequence of resulting NMR spectra is shown in Fig. 6 (a). For strong external fields with $\eta \geq 0.2$ the Pake-type pattern transforms into a spectrum with two narrow peaks and this indicates that for $\eta \geq 0.2$ most of the molecules are aligned along $\mathbf{f}$, except for those lying close enough to the polymer substrate.

To gain more insight into field-induced changes of NMR spectra, it is convenient to investigate nematic ordering layer by layer [5] from the center towards the droplet surface, calculating the local nematic order

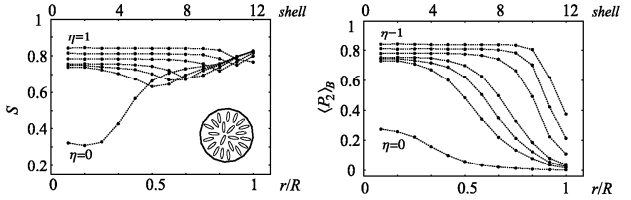

Figure 7. Order parameters calculated for the radial droplet at $T^* = 0.8$ (nematic phase). Local nematic (S, *left*) and external field ($\langle P_2\rangle_B$, *right*) order parameter as a function of the distance from the droplet center. Curves are plotted for (top to bottom): $\eta = 1$, 0.5, 0.2, 0.05, 0.03, 0.02, and 0, respectively. The defect core transforms into an aligned structure. The molecular alignment for $\eta = 0$ is depicted schematically as inset.

parameter S and the external field order parameter $\langle P_2\rangle_B$. Recall that the parameter S gives information on the degree of nematic ordering with respect to the average local molecular direction (the local director $\mathbf{n}$). The parameter $\langle P_2\rangle_B$, however, is defined as $\langle P_2\rangle_B = \langle \frac{1}{2}(3\cos^2\beta_i - 1)\rangle_i$, with $\cos\beta_i = \mathbf{f}\cdot\mathbf{u}_i$ and the brackets $\langle ...\rangle_i$ representing the time and ensemble average over orientations of molecules (spins) within a given spherical layer. Contrary to S, $\langle P_2\rangle_B$ contains information on molecular ordering along a fixed direction — determined by the external field — and thereby reflects also spatial variations of the nematic director. Note also that the number of spins within a certain shell increases rapidly when moving from the droplet center towards the surface (from 8 spins in the central shell to 1392 spins in the outermost shell). The maximum variance of S (up to 6% in the bipolar and up to 30% in the radial case), however, usually occurs in intermediate shells or even close to the substrate. In these regions the aligning effects of the substrate conflict either with the ordering effect of the external field or with the parallel aligning tendency of the nematic-nematic interaction. The competition of these effects may result also in a slight decrease of S. A calculation of the parameter S (Fig. 7, left) for $\eta = 0$ shows that the value of S in the center of the droplet is nonzero but considerably smaller (≈ 0.32) than the value obtained in the intermediate and surface layers (more than ≈ 0.75). This confirms the existence of a small (~ 4 molecular or "cluster" dimensions diameter) and fairly disordered defect core.

Increasing the field strength, the degree of ordering in the center increases significantly and the molecules of the core align along the field direction (compare with order parameters S and $\langle P_2\rangle_B$ plotted in Fig. 7). There is no critical field characterizing the transition between the "hedgehog" and the aligned structure: the size of the aligned core increases gradually with the increasing field strength [6]. At the same time, surface-inducedradial order persists in the outermost molecular layers, which results in a strong decrease of the order parameter $\langle P_2\rangle_B$ (Fig. 7, right) in the surface region. The thickness of this region is again roughly equal to the field coherence length ξ. In the intermediate regime with $0 < \eta < 0.2$ the spectra are composed both of the Pake type contribution originating from the surface layers and of two narrow peaks being a signature of the field-ordered core. With increasing η the latter contribution prevails, as it is clearly evident from Fig. 6 (a). It is possible to check the agreement of values for S deduced from peak positions and from MC data [16].

In the fast diffusion regime the spectrum of the radial droplet for $\eta = 0$ consists of a single line located at $\langle\omega_Q\rangle = 0$ since the molecular orientational distribution is spatially isotropic [11]. As soon as there is a preferred direction (like in a strong field), $\langle\omega_Q\rangle = 0$ no longer holds and the spectrum splits into two narrow and symmetric peaks. Fig. 6 (b) shows the fast diffusion spectra for radial boundary conditions. As expected, we observe a single line in the spectrum only if the external field is off or relatively weak with $\eta \leq 0.02$. Increasing the field strength, the spectrum gradually transforms into the two-peak pattern described above. The comparison of peak positions and $\langle\omega_Q\rangle$ calculated from MC data gives a fairly good agreement of the two estimates.

4.2 Bipolar droplet

In the bipolar droplet the local anchoring easy axis is directed tangentially to the local droplet surface, while it is also lying in a plane containing the droplet symmetry axis. Suppose also that the directions of the NMR spectrometer field and of the external field match with the symmetry axis of the droplet, here denoted by z. For all droplets in a real PDLC sample this can be achieved by applying an external magnetic field of sufficient strength during the droplet formation process [11]. Consider again the limit without translational diffusion and assume also that there is no external field applied ($\eta = 0$), except for the weak spectrometer field that anyway does not disturb the nematic director configuration. Again, the reduced temperature was set to $T^* = 0.8$. The results show that a considerable portion of nematic molecules — especially those in

the droplet core — is directed approximately along the spectrometer field, which results in a spectrum consisting of two well-defined peaks [Fig. 8 (a)] situated almost at maximum quadrupolar splitting $\delta\omega_Q$, reduced by the factor S due to fluctuations of molecular long axes [see Eq. (5)]. These peaks are located at $\omega_Q/\delta\omega_Q \approx \pm(0.73 \pm 0.01)$, which roughly suggests that $S \approx 0.73$. Unless noted otherwise, the error in S arising from the determination of peak positions in all following cases equals ± 0.01. It is interesting to notice that the determination of S directly from MC data yields $S \approx 0.76 \pm 0.04$ and then the agreement of the two estimates is rather good.

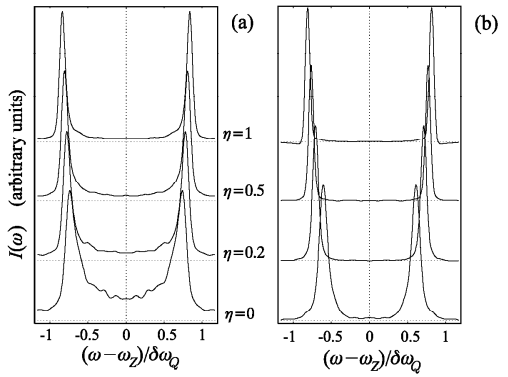

Figure 8. ^{2}H NMR spectra of the bipolar droplet in the nematic phase at $T^* = 0.8$ for different values of the external field strength ($\propto \sqrt{\eta}$); no-diffusion limit (a), fast diffusion limit (b). The quadrupolar splitting increases with increasing η. All spectra have been normalized so as to obtain same peak heights.

Increasing now the external field strength to yield $\eta - 0.2$, the two peaks in the spectrum move towards larger $|\omega_Q|$, i.e., to $\omega_Q/\delta\omega_Q \approx \pm 0.78$ and become narrower. The MC data now yield $S \approx 0.79 \pm 0.03$. As it is evident from Fig. 8 (a), this trend continues also in even stronger fields with $\eta = 0.5$ ($\omega_Q/\delta\omega_Q \approx \pm 0.81$) and $\eta = 1.0$ ($\omega_Q/\delta\omega_Q \approx \pm 0.84$). The corresponding MC-data values for S are then 0.81 ± 0.02 and 0.84 ± 0.015, agreeing perfectly with the values deduced from the spectra. Note that already for $\eta = 0.2$ the external field is extremely strong: considering the magnetic case and taking $\epsilon = k_B T_{NI}/1.1232 \approx 0.023$ eV (with $T_{NI} \approx$

300 K), the macroscopic anisotropy of the magnetic susceptibility $\chi_a S \approx 10^{-6}$, and assuming a single spin to represent a cluster of up to 100 nematic molecules of volume 1 nm^3 each, we obtain as much as $B \approx 150$ T. If we used an electric instead of the magnetic field to align the nematic, the corresponding field strength for a typical liquid crystal with $\epsilon_a S \approx 1$ and for same η would be ≈ 45 V/μm, which is — like in the magnetic case — rather difficult to be implemented experimentally. It must be stressed, however, that strong external fields are required to induce a detectable distortion because the simulated droplet is still rather small and because surface anchoring was chosen strong [16].

The S-profiles for the bipolar droplet in the nematic phase for $T^* = 0.8$ are displayed in Fig. 9, left. They indicate that the degree of nematic ordering is almost constant throughout the droplet core with $S \approx 0.74$ when the external field is absent, while it increases to $S \approx 0.82$ in the surface layer due to ordering effects of the polymer substrate. Applying the field, the degree of molecular order inside the core increases, if compared to the case without field; e.g., for $\eta = 1$ even to $S \approx 0.84$. The profiles of the field order parameter $\langle P_2 \rangle_B$ are plotted in Fig. 9, right. The corresponding curve for $\eta = 0$ shows that already in absence of the field there is net molecular alignment along the z-axis, which agrees with the imposed bipolar boundary conditions whose symmetry axis matches with z. The curves for $\eta > 0$ show that with the increasing field strength more and more molecules (spins) orient along z (i.e., along $\mathbf{f}$), thereby increasing the size of the droplet core where the nematic liquid crystal is almost undistorted and $\mathbf{n}||z$. The thickness of the distorted region is related to the external field coherence length ξ and is obviously microscopic because the applied field is extremely strong.

According to the above observations, the increase of the quadrupolar splitting ω_Q in strong fields can be attributed both to the overall increase in the local degree of ordering, i.e., to an increase of S — as observed also experimentally [30] —, and to the additional molecular alignment along $\mathbf{f}$ resulting in an increase of $\langle P_2 \rangle_B = \langle P_2(\cos\theta) \rangle$; see Eq. (5). Also the narrowing of the spectral lines is related to the increase of $\langle P_2 \rangle_B$ since in the droplet core the bipolar configuration is replaced by the "aligned" one. The spectral line narrowing further follows from changes in the distribution of local $S(\mathbf{r})$. In fact, in strong fields the field-enhanced "bulk" value of S approaches the surface-induced value and thus the distribution of S becomes narrower.

Considering now Fig. 8 (b) and the spectra of bipolar droplets in the fast translational diffusion limit (or, equivalently, in small enough nematic droplets), the spectra for all η still consist of two well-defined lines now positioned, however, at an average quadrupolar frequency given by

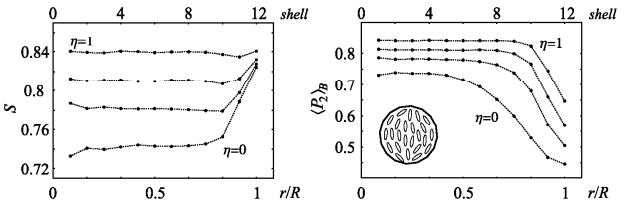

Figure 9. Order parameters calculated for the bipolar droplet at $T^* = 0.8$ (nematic phase): local nematic (S, *left*) and external field ($\langle P_2 \rangle_B$, *right*) order parameter as a function of the distance from the droplet center. Curves are plotted for (top to bottom): $\eta = 1$, 0.5, 0.2, and 0, respectively. External field enhances the degree of nematic ordering (*left*) and increases the size of the aligned core (*right*). The molecular alignment for $\eta = 0$ is depicted schematically as inset.

$\langle \omega_Q \rangle = \pm \delta\omega_Q \langle \frac{1}{2} [3(\mathbf{u}_i \cdot \mathbf{B}_0/B_0)^2 - 1] \rangle_i$, where $\langle ... \rangle_i$ represents the average over fluctuations and diffusive motions of all molecules within the PDLC droplet [11]. The quantity $\langle \omega_Q \rangle$ can be calculated also directly from MC data and the agreement with actual peak positions is very good.

5. Many-droplet sample

All the cases treated so far concerned only a single PDLC droplet. In a real sample, however, there are many droplets, all of them contributing to the macroscopic response of the system. In the following we will focus on a system of many bipolar droplets, with their symmetry axes oriented randomly. Macroscopically, such a sample behaves as isotropic although the constituent bipolar droplets are not. Then, in the spectrum (representing the collective response from all droplets) one should expect to see the Pake-type pattern — characteristic for isotropic orientational distributions — instead of the two-peaked spectrum obtained for a single droplet. In an experiment, the two-peaked spectrum can be obtained only if all bipolar symmetry axes are preliminarily aligned by a strong external electric or magnetic field.

Although we only have the MC data for one droplet available, the individual droplets in the PDLC sample act independently and thus it is possible to simulate the effect of randomly oriented droplet symmetry axes by using the unaltered single droplet data and by assuming to have

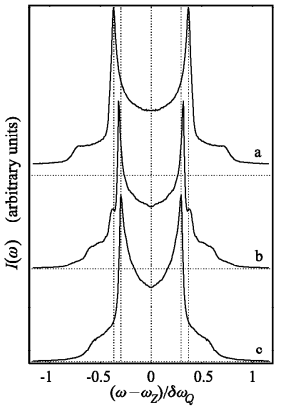

Figure 10. Spectra of 1000 bipolar droplets at $T^* = 0.8$, with symmetry axes oriented randomly: no diffusion (a), fast diffusion: inhomogeneous (b) and homogeneous (c).

a random distribution of spectrometer magnetic field directions [21]. Since we simply "clone" the data for a single droplet to model several droplets, this certainly results in unphysical correlations between particle orientations in different droplets, but at least in cases with diffusion this should not be of great importance since inter-droplet correlations are smeared out by independent diffusion paths in each droplet. Note that now spectra show much less noise than for a single droplet and it is not necessary to perform smoothening convolutions.

Fig. 10 (a) shows the spectrum of 1000 bipolar droplets without diffusion at $T^* = 0.8$ (nematic phase). It presents a Pake-type pattern, as expected, with peaks positioned at $\pm 0.37\,\delta\omega_Q$. This suggests that $S \approx 0.74$, which is close to $S \approx 0.73$, a value deduced from peak positions for a single bipolar droplet. In the spectrum, fast and homogeneous diffusion again results in a Pake-type pattern [Fig. 10 (c)]. The ratio of line widths measured peak-to-peak in cases with and without fast diffusion should be equal to that calculated for a single bipolar droplet. For a single droplet this ratio is estimated by 0.83, while for an array of 1000 droplets we have 0.80, indicating that the agreement is good.

However, as suggested by experimental results, in a thin subsurface layer molecular diffusive motion is hindered, which results in a signif-

icant reduction of the effective diffusion constant D (even by a factor of 3×10^3) [29]. Simulating diffusion, we decided to take into account also this slow-down effect, setting the thickness of the subsurface layer to roughly one particle dimension (up to ~ 5 nm), thereby leaving 1608 particles (out of 5832) in the subsurface region. Then the rate of diffusive moves within this region was reduced and the same reduction factor was assumed also for moves entering or leaving the surface layer. Inspecting the resulting spectrum [Fig. 8 (b)], it is still similar to the Pake-type pattern, however, with less width reduction than in the homogeneous diffusion case. In addition, at splittings slightly larger than those corresponding to the main peaks, two "shoulders" appear. The spectrum shown in Fig. 10 (b) actually consists of two super-imposed Pake-type patterns. The first one — comprising the two main peaks — is well-pronounced and originates from central droplet regions where diffusion is effective. The two "shoulders", on the other hand, are the main peaks of the less pronounced, but not diffusion-narrowed second Pake-type pattern representing the response from droplet surface layers. Note that the "shoulder" and no-diffusion peak positions [Fig. 10 (a)] match again.

6. Conclusions

We have described lattice spin models for the simulation of polymer-dispersed liquid crystals. The biggest advantage of Monte Carlo simulations is the possibility of investigating the system at a microscopic level, and to calculate thermodynamic properties and their specific order parameters suitable for different types of PDLC. Molecular organizations can be investigated by calculating the order parameters point by point across the droplet. Moreover, it is possible to calculate experimental observables like optical textures and, as discussed here, ^{2}H NMR line shapes. We have given an overview of the method and some applications to models of PDLC with radial and bipolar boundary conditions, and considered the effect of orientational and translational diffusion on the spectra. We have examined in particular under what conditions the NMR spectra of the deuterated nematic can provide reliable information on the actual boundaries present in these submicron size droplets.

Acknowledgments

The authors wish to thank EU through TMR FULCE "*Functional Liquid–Crystalline Elastomers*", contract HPRN-CT-2002-00169, for financial support.

References

[1] P. Pasini and C. Zannoni (eds.), *Advances in the Computer Simulations of Liquid Crystals*, Kluwer, Dordrecht (2000).

[2] P. A. Lebwohl and G. Lasher, *Phys. Rev. A*, 6:426 (1972).

[3] J. G. Gay and B. J. Berne, *J. Chem. Phys.*, 74:3316 (1981).

[4] C. Zannoni, *J. Mater. Chem.*, 11:2637 (2001).

[5] C. Chiccoli, P. Pasini, F. Semeria, and C. Zannoni, *Phys. Lett. A*, 150:311 (1990); *Mol. Cryst. Liq. Cryst.*, 221:19 (1992).

[6] E. Berggren, C. Zannoni, C. Chiccoli, P. Pasini, and F. Semeria, *Chem. Phys. Lett.*, 197:224 (1992); *Phys. Rev. E*, 49:614 (1994); *Phys. Rev. E*, 50:2929 (1994); *Mol. Cryst. Liq. Cryst. A*, 266:241 (1995).

[7] G. P. Crawford and S. Žumer, *Liquid Crystals in Complex Geometries Formed by Polymer and Porous Networks*, Taylor and Francis, London (1996).

[8] M. Ambrožič, P. Formoso, A. Golemme, and S. Žumer, *Phys. Rev. E*, 56:1825 (1997).

[9] N.D. Mermin, *Rev. Mod. Phys.*, 51:591 (1976).

[10] O.D. Lavrentovich, P. Pasini, C. Zannoni, and S. Žumer (eds.), *Defects in Liquid Crystals: Computer Simulations, Theory and Experiments*, Kluwer, Dordrecht (2001).

[11] A. Golemme, S. Žumer, J. W. Doane, and M. E. Neubert, *Phys. Rev. A*, 37:559 (1988).

[12] R. Ondris-Crawford, E. P. Boyko, B. G. Erdmann, S. Žumer, and J. W. Doane, *J. Appl. Phys.*, 69:6380 (1988).

[13] P. Drzaic, *Mol. Cryst. Liq. Cryst.*, 154:289 (1988).

[14] R. Aloe, G. Chidichimo, and A. Golemme, *Mol. Cryst. Liq. Cryst.*, 203:1155 (1991).

[15] C. Chiccoli, P. Pasini, G. Skačej, C. Zannoni, and S. Žumer, *Phys. Rev. E*, 60:4219 (1999).

[16] C. Chiccoli, P. Pasini, G. Skačcj, C. Zannoni, and S. Žumer, *Phys. Rev. E*, 62:3766 (2000).

[17] U. Fabbri and C. Zannoni, *Mol. Phys.*, 58:763 (1986).

[18] Z. Zhang, O. G. Mouritsen, and M. Zuckermann, *Phys. Rev. Lett.*, 69:2803 (1992).

[19] N. Metropolis, A. W. Rosenbluth, M. N. Rosenbluth, A. H. Teller, and E. Teller, *J. Chem. Phys.*, 21:1087 (1953).

[20] J. H. Barker and R. O. Watts, *Chem. Phys. Lett.*, 3:144 (1969).

[21] C. Chiccoli, P. Pasini, G. Skačej, C. Zannoni, and S. Žumer, *Mol. Cryst. Liq. Cryst.*, 367:199, (2001).

[22] C. Chiccoli, P. Pasini, F. Semeria, T. J. Sluckin, and C. Zannoni, *J. de Physique II*, 5:427 (1995).

[23] A. Golemme, S. Žumer, D. W. Allender, and J. W. Doane, *Phys. Rev. Lett.*, 61:2937 (1988).

[24] J. Dolinšek, O. Jarh, M. Vilfan, S. Žumer, R. Blinc, J. W. Doane, and G. Crawford, *J. Chem. Phys.*, 95:2154 (1991).

[25] A. Abragam, *The Principles of Nuclear Magnetism*, Clarendon Press, Oxford (1961).

[26] R. Y. Dong, *Nuclear Magnetic Resonance of Liquid Crystals*, Springer-Verlag, New York (1994).

[27] S. Žumer, P. Ziherl, and M. Vilfan, *Mol. Cryst. Liq. Cryst.*, 292:39 (1997).

[28] P. G. de Gennes and J. Prost, *The Physics of Liquid Crystals*, Clarendon Press, Oxford (1993).

[29] G. P. Crawford, D. K. Yang, S. Žumer, D. Finotello, and J. W. Doane, *Phys. Rev. Lett.*, 66:723 (1991).

[30] I. Lelidis, M. Nobili, and G. Durand, *Phys. Rev. E*, 48:3818 (1993).